SUPERCRITICAL FLUID REACTIONS FOR COAL PROCESSING

FINAL TECHNICAL REPORT

Period Covered by Report: September 1, 1994 – August 31, 1997

Principal Investigator:
Professor Charles A. Eckert

Report Issued: November, 1997

DOE Award No.: DE-FG22-94PC94206--13

Submitting Organization:

Georgia Institute of Technology
School of Chemical Engineering
778 Atlantic Ave.
Atlanta, GA 30332-0100

Disclaimer

Exciting opportunities exist for the application of supercritical fluid (SCF) reactions for the pre-treatment of coal. Utilizing reactants which resemble the organic nitrogen containing components of coal, we developed a method to tailor chemical reactions in supercritical fluid solvents for the specific application of coal denitrogenation. The tautomeric equilibrium of a Schiff base was chosen as one model system and was investigated in supercritical ethane and cosolvent modified supercritical ethane. The Diels-Alder reaction of anthracene and 4-phenyl-1,2,4-triazoline-3,5-dione (PTAD) was selected as a second model system, and it was investigated in supercritical carbon dioxide.

TABLE OF CONTENTS

LIST OF GRAPHICAL MATERIALS

EXECUTIVE SUMMARY

Exciting opportunities exist for the application of supercritical fluid (SCF) reactions for the pre-treatment of coal. Utilizing reactants which resemble the organic nitrogen containing components of coal, we developed a method to tailor chemical reactions in supercritical fluid solvents for the specific application of coal denitrogenation. The tautomeric equilibrium of a Schiff base was chosen as one model system and was investigated in supercritical ethane and cosolvent modified supercritical ethane. The Diels-Alder reaction of anthracene and 4-phenyl-1,2,4-triazoline-3,5-dione (PTAD) was selected as a second model system, and it was investigated in supercritical carbon dioxide.

INTRODUCTION

The goal of this work is to develop benign solvent/cosolvent systems for reactions which will achieve optimum denitrogenation in the pretreatment of coal or coal liquids. Supercritical fluids present excellent opportunities for the pre-treatment of coal, hence we shall utilize supercritical fluids as a reaction medium. A SCF exists in a single phase just above the critical temperature at elevated pressures. It has a liquid-like density, which gives a large capacity for solvation, and it has a high molecular diffusivity and low viscosity, which makes it an ideal medium for efficient mass transfer. Further, its high compressibility gives large density variations with very small pressure changes, yielding extraordinary selectivity characteristics, which are most important in the removal of nitrogen from coal or coal liquids. Significant work has already been carried out in such applications, both in general (Johnston, 1989; Ely, 1991; Brennecke, 1989), as well as in many specific applications to environmental control (Leman, 1990; Eckert, 1986).

There are four specific objectives of this work. First is the use of supercritical fluids and modified supercritical fluids to tune the chemical equilibria of model coal compounds. A second objective is to model the density dependence of the equilibrium constant using a chemical-physical approach. Third is the quantification of the intermolecular interactions affecting reaction transition states in SCFs via kinetic measurements using well-characterized Diels-Alder reactions. The final objective is the characterization of the thermodynamics of the reacting systems. From the thermodynamics of the reacting species, detailed information about the transition state may be determined.

BACKGROUND

A great deal of theoretical work has been done toward rate predictive models capable of correlating rate constant data versus various solvent properties and thermodynamic variables. A review of this broad field of research is beyond the scope of this work, but a thorough discussion is provided in reviews by Savage and Clifford (Clifford and Bartle, 1996; Savage, et al., 1995). For the present purpose, an overview of the most important concepts will suffice as an introduction to ways in which the data in this work could be employed in future modeling efforts.

Arrhenius Activation Energy

The most traditional method of analyzing rate data is in terms of the Arrhenius equation, which is presented as equation (1). The Arrhenius equation represents the exponential relationship between rate constant and temperature, and can be used to extract information on the activation energy, which is defined as the energy needed to bring one mole of reactants from the ground state to the transition state of the reaction (Laidler, 1987a).

$$k_c = k_o e^{\left(-\frac{E_a}{RT}\right)} \qquad (1)$$

Solvent effects may be quantified using this relationship by determining the changes in activation energy that occur with changes in solvent properties (Hughes and Ingold, 1935, Tester, 1996). A solvent's effect on reaction rate is then discussed in terms of its ability to stabilize the transition state (Laidler, 1987b). Stabilization of the transition state through changes in solvent environment produces a lower energy of activation and a

faster reaction. Prediction of solvent effects on reaction rates is accomplished through a linear correlation of the log of the rate constant, which is proportional to the activation energy, versus an appropriate solvent property. Examples of solvent properties against which correlations can be made include density, dielectric constant, or a solvatochromic parameter such as α, which measures a solvent's hydrogen bond donating ability; β, which measures hydrogen bond accepting ability; or π^*, which measures polarity/polarizability (Kim and Johnston, 1987a). A drawback of this method is that a large amount of experimental rate data needs to be collected in order to apply the technique. The data must cover a wide range of solvent types and reaction conditions before solvent effects can be predicted for an uncorrelated solvent. Even if the necessary data are available, the reaction rate predicted for the new solvent may possess significant error due to unusual specific interactions between solvent and reactants.

Transition State Theory

A more rigorous approach to the prediction of solvent effects on reaction rate is provided by transition state theory. In this treatment, it is assumed that the rate of reaction is dependent on an equilibrium established between the two reactant molecules and an "activated complex".

$$A + B \leftrightarrow M \leftrightarrow \text{Products}$$

The activated complex M is formed from the association of two reactant molecules A and B as bonds are broken and formed on the way to product. Though the activated complex is unstable along the reaction coordinate, it is considered to be a normal molecule in equilibrium with the reactants and may therefore be used in writing relationships based on thermodynamic activities (Eckert, 1967; Evans and Polanyi, 1935; Eyring, 1935).

$$K_{eq} = \frac{[M]}{[A][B]} \frac{\gamma_M}{\gamma_A \gamma_B} \qquad (2)$$

Equation (2) was related to chemical reaction rates by Bronsted and Bjerrum (Bjerrum, 1924; Bronsted, 1922), producing a general statement which relates the reaction rate constant to solvent effects through activity coefficients.

$$k = k_o \frac{\gamma_A \gamma_B}{\gamma_M} \qquad (3)$$

In equation (3), the rate constant k is a product of k_o, the rate constant in a standard state environment (where all activities are unity), and the activity coefficients of the reactants and activated complex at the actual conditions of the reaction. This relationship cannot predict absolute reaction rates, but does have the potential to predict changes in the rate constant with a change in reaction conditions. The ability of this relationship to predict reaction rates relative to the rate at a standard state is limited only

by the validity of the solution theory used to define the activity coefficients. If a solution theory possessing a small number of adjustable parameters is applicable to a given reaction, transition state theory has the potential to provide solvent effect predictions with less data than correlations based on Arrhenius activation energies.

Scatchard and Hildebrand's regular solution theory estimates activity coefficients for an ideal system in which only dispersion forces need be considered, so it can be used to provide a simple example of how (3) can be modified for practical application (Hildebrand and Scott, 1962; Hildebrand, 1964 #105). In the Scatchard and Hildebrand model, a solubility parameter, δ, is defined for the solvent and for each reactant, based on the "cohesive energy density" of the material - an experimentally measurable value that represents the strength of dispersion forces as the energy needed to isothermally vaporize a given molar volume of liquid to the ideal gas state. When δ is related to the activity of a component, the following simple relationship results.

$$RT \ln \gamma_j = v_j \left(\delta_j - \bar{\delta} \right)^2 \qquad (4)$$

$$\bar{\delta} \equiv \sum_i^m \Phi_i \delta_i \qquad (5)$$

Substitution into (3) leads to the following useful result. Note that for work done with dilute reactants, $\bar{\delta}$ is approximately equal to the solubility parameter of the solvent δ_S.

$$\ln\left(\frac{k}{k_O}\right) = \frac{v_A\left(\delta_A - \delta_S\right)^2 + v_B\left(\delta_B - \delta_S\right)^2 - v_M\left(\delta_M - \delta_S\right)^2}{RT} \qquad (6)$$

Local Density Enhancement

The rate predictive model based on regular solution theory would probably not work in the near critical region of a solvent, due to the tendency of a near critical solvent to exhibit densities in the vicinity of the reactants that are higher than the density of the bulk fluid. This local density enhancement represents a significant change in solvent properties unrelated to dispersion forces, and the regular solution theory based model would fail to account for its effects.

Local density enhancement is brought about by short-range solute-solvent interactions at solvent densities between 0.4 and 0.8 times the critical density (Brennecke, et al., 1990; Eckert and Knutson, 1993; Kim and Johnston, 1987b; Paulaitis and Alexander, 1987). Local density enhancement has the effect of creating local or "true" reactant concentrations which differ from the concentrations found in the bulk fluid.

Local density enhancements have been investigated using a solvatochromic method which correlates shifts in the transition energy of spectroscopic absorption maxima to changes in density in the immediate vicinity of a probe molecule. This provides a means of measuring density enhancements in a supercritical solvent, and subsequently correcting

measured rate constants for these enhancement effects (Kim and Johnston, 1987a). Application of this method to an esterification reaction in supercritical CO_2, for example, suggests that, in at least some cases, changes in the rate constant near the critical pressure may be explained largely by the effect of density enhancement on local concentration, rather than by physical or thermodynamic effects (Brennecke, et al., 1994).

In conclusion, solvent characteristics peculiar to supercritical fluids, such as local density enhancement and high solvent compressibility near the critical point, present challenges to those who wish to develop predictive models of chemical reaction rates in supercritical solvents. A number of general theories capable of predicting solvent effects on reaction rates already exist. The challenge is to incorporate expressions which account for supercritical fluid solvent properties into these theories.

RESULTS AND DISCUSSION

I) TAUTOMERIC EQUILIBRIUM OF A SCHIFF BASE

Keto-Enol Equilibrium Measurements

Recent studies of chemical equilibria have focused on the effects of pressure on the equilibrium constants of solutes in pure supercritical fluids (Yagi, 1993; Kazarian, 1993; Yamasaki, 1990). The presence of a cosolvent complicates the system, especially if the cosolvent is capable of participating in specific interactions with the solute molecule and leads to multiple equilibria. However, it is the purpose of this study to quantify the effect of cosolvents on keto-enol equilibrium constant for the Schiff base, 4-(methoxy)-1-(N-phenylforminidoyl)-2-naphthol (Figure 1), especially in the near-critical region where local composition enhancements are expected to have a large effect on the equilibrium constant.

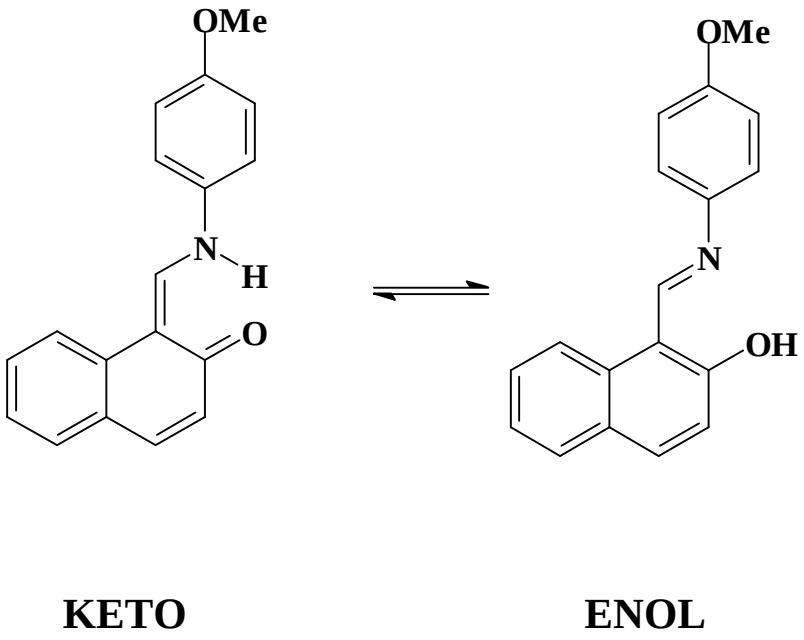

Figure 1. Tautomeric equilibrium of the Schiff base 4-(methoxy)-1-(N-phenylforminidoyl)-2-naphthol.

The Schiff base and a blocked Schiff base (Figure 2) were synthesized by a condensation reaction of 2-hydroxynaphthaldehyde and p-methoxy aniline in ethanol

(Salman, 1991) and by a condensation reaction of 2-methoxy-1-naphthaldehyde and 4-methoxyaniline in ethanol, respectively. Yellow solids of blocked Schiff base were obtained after filtration, washing twice with cold ethanol and drying under vacuum. ^{1}H NMR ($CDCL_3$ and TMS): δ = 3.78 ppm (s, 3H); 6.94 ppm (d, 2H); 7.18 ppm (d, 1H); 7.30 ppm (d, 2H); 7.36 ppm (m, 1H); 7.56 ppm (m, 1H); 7.74 ppm (d,1H); 7.85 ppm (d, 1H); 9.25 ppm (s, 1H); 9.53 ppm (d, 1H); 13C NMR ($CDCl_3$ and TMS): δ = 55.30 ppm (s); 56.26 ppm (s); 112.53 ppm (s); 114.38 ppm (s); 117.37 ppm (s); 122.30 ppm (s); 124.23 ppm (s); 126.07 ppm (s); 128.29 ppm (s); 128.40 ppm (s); 129.26 ppm (s); 132.05 ppm (s); 133.39 ppm (s); 146.61 ppm (s); 157.02 ppm (s); 158.22 ppm (s); 159.31 ppm (s). The blocked Schiff base had the phenolic oxygen methylated to prohibit tautomerization so that the extinction coefficients of the enol form of the Schiff could be measured.

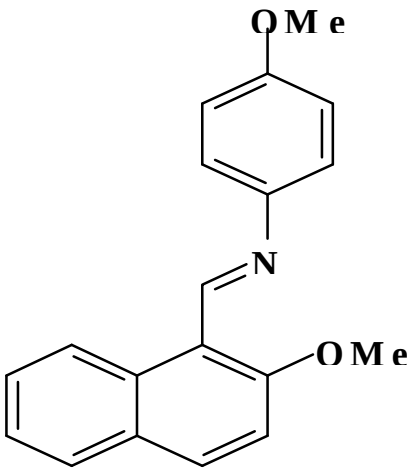

Figure 2. Blocked Schiff base.

Apparatus

A schematic of the modified UV spectrophotometer (Perkin Elmer 554) is shown in Figure 3. Single beam spectroscopy was used in this double beam apparatus using air as a constant background for enhanced signal to noise ratio. The spectrophotometer was modified to accommodate a stainless steel high pressure cell (Tomasko, 1992) with quartz windows (Heraeus Amersil). The path length of the cell was 0.75 cm and the volume was 5.88 ml. The cell was stirred continuously using a mini stir plate (Variomag) and a stir bar (Fisher) placed inside the cell.

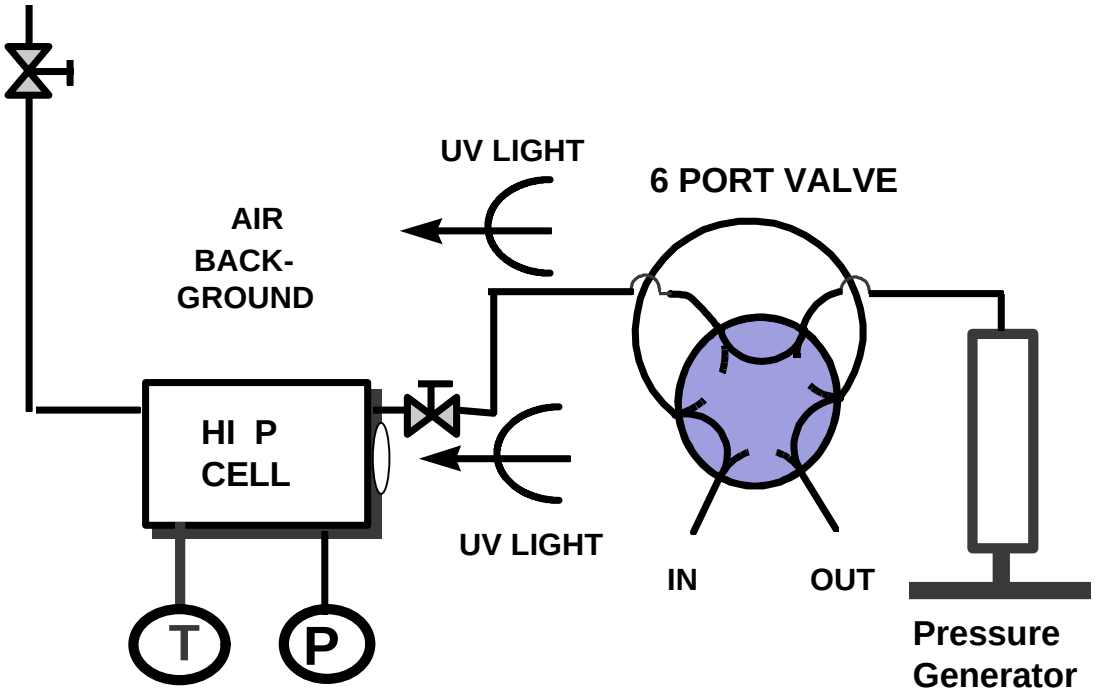

Figure 3. Schematic diagram of high pressure UV-Vis reaction apparatus.

The temperature inside the cell was monitored with an internal thermistor (Omega, calibrated within ± 0.1°C) and controlled manually using an EPSCO DC power supply (Model D-612T). Heat was supplied by thermoelectric heaters (Melcor). The pressure was controlled using a 60 cm^3 piston type high pressure generator (High Pressure Equipment, Model 87-6-5) and measured to within ± 2 psi with a Heise digital pressure gauge (Model 901B). A Valco 6-port sampling valve with external sample loops ranging in size from 20-100µl was used to inject cosolvent directly into the high pressure cell.

Procedure

Single beam spectroscopy was used to monitor absorbance as a function of increasing pressure at constant probe and cosolvent concentrations. All measurements were made at a constant temperature of 35°C (± 0.1°C), and all experiments were carried out in the single phase region, as confirmed by separate miscibility experiments (Yun, 1996) (Table 1).

Table 1. Pressure limits of miscibility for SCF ethane/cosolvent mixtures.

Cosolvent in SCF Ethane	Cosolvent Concentration (mol/L)	Lower Miscibility Limit (psig)
Trifluoroethanol	0.24	800
Trifluoroethanol	0.12	756
Trifluoroethanol	0.046	738
Hexafluoroiso-propanol	0.32	721
Hexafluoroiso-propanol	0.16	713
Hexafluoroiso-	0.08	Miscible at all conditions

propanol		observed.
Ethanol	0.2	Miscible at all conditions observed.
Ethanol	0.1	Miscible at all conditions observed.

Spectra at different pressures were recorded, starting with a low pressure as determined by the miscibility limit, and incrementally going to higher pressures. The absorbance was recorded at the wavelength of maximum absorption for each tautomer at least three times to obtain an average value (standard error ± 2% at higher pressures; ± 5% at pressures below 730 psig). The pressure varied less than 1.5 psi within a single spectral scan, and data were taken with increasing pressure to ensure that the solute concentration remained constant. Since single beam spectroscopy was used in this double beam apparatus, blank runs (no Schiff base) were made for each solvent system at every pressure point, and this subsequent spectrum was subtracted from the spectrum which contained the Schiff base.

The high-pressure cell was loaded with a solution of 20 μl of (0.0437 M) Schiff base in acetone using a syringe to obtain a probe concentration of 1.5×10^{-4} M, which is below the solubility limit at experimental conditions as determined spectroscopically. The cell was flushed with multiple volumes of low pressure ethane to evaporate the acetone and to displace air from the system. In the experiments without cosolvent, the cell was then pressurized with ethane to the desired initial pressure. In cases where cosolvent was added, the cell was charged with 100 psig of ethane after removing air from the system. Then, the cell was isolated from the rest of the system, and the lines leading to the cell

were pressurized with 450 psig of ethane. The external sample loop was then rinsed and filled with the cosolvent, and the sampling valve and the valve leading to the cell were opened simultaneously to force the cosolvent into the cell using the pressure differential. The cell was further pressurized with ethane to the desired pressure set point, and after equilibration of temperature and pressure, absorbance spectra were measured as described above.

Calculation of K_C

The equilibrium constant (K_C) was calculated from the following equation:

$$K_c = \frac{c_{keto}}{c_{enol}} \qquad (1)$$

where c_{keto} is the concentration of the keto tautomer and c_{enol} is the concentration of the enol tautomer. Concentration is related to the measured absorbance through Beer's law, thus,

$$K_c = \left(\frac{\varepsilon_{enol}}{\varepsilon_{keto}}\right)\left(\frac{A_{\lambda_{\max,keto}}}{A_{\lambda_{\max,enol}}}\right) \qquad (2)$$

where A represents the absorbance at the maximum wavelength for each tautomer for a given solvent system. The ratio of extinction coefficients and absorbances were obtained as described previously. The wavelength of maximum absorption changes for the various cosolvent modified SCF solutions due to solvochromatic shifts.

Results and Discussion

The experimental equilibrium constant was found to be a function of cosolvent acidity, cosolvent concentration, and density. Polar cosolvents such as acetone, chloroform, and dimethylacetamide (DMA) did not affect the position of tautomeric equilibria. Only cosolvents capable of hydrogen bonding (EtOH, TFE, and HFIP) led to any significant amount of Schiff base tautomerization; the equilibrium constant shifted towards the keto tautomer in the presence of cosolvents which were capable of forming hydrogen bonds. The equilibrium constant also increased with increasing acidity of the cosolvent as can be seen in Figure 4.

The equilibrium constant was also found to shift substantially with varying amounts of cosolvents as can be seen in Figure 5 with the TFE modified SCF ethane solvent system.

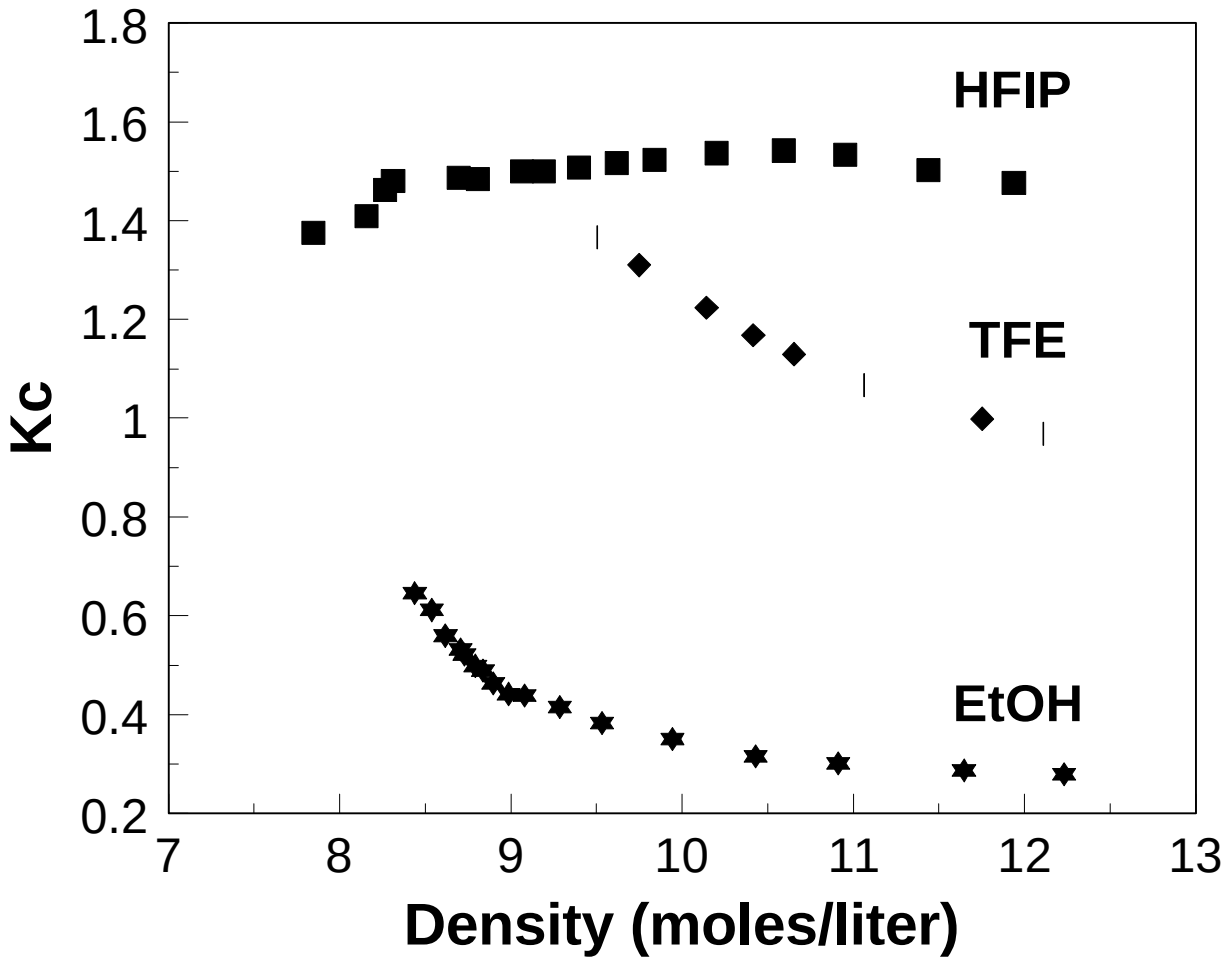

Figure 4. Equilibrium constant (K_c) as a function of density for approximately 0.1 M cosolvent (EtOH, TFE, HFIP) in SCF ethane. (Equilibrium constant (K_c) as a function of density for approximately 0.1 M cosolvent in SCF ethane.)

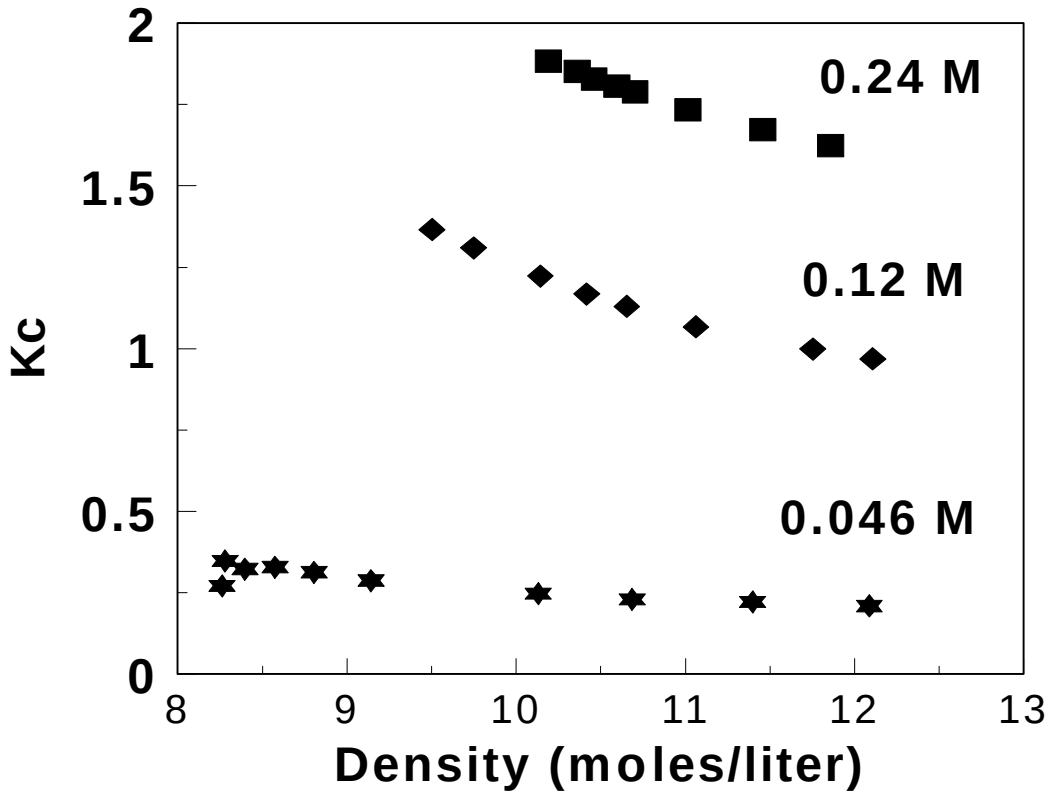

Figure 5. Equilibrium constant (K_c) as a function of density for 0.046 M, 0.12 M, and 0.24 M TFE in SCF ethane. (Equilibrium constant (K_c) as a function of density for Schiff base in TFE modified SCF ethane.)

It is important note that miscibility limits and critical mixture densities are different for each cosolvent system and for each cosolvent concentration; therefore, experimental data do not all begin at the same density. The same trend of shift in equilibrium constant was also found with ethanol and HFIP as cosolvents.

These results indicate large changes in tautomerization equilibrium may be obtained with small amounts of carefully selected cosolvents; however, the most interesting and informative result is the variation of the equilibrium constant with density. This effect can be seen in Figure 6 for ethanol and TFE modified SCF ethane solvent

systems. The ethanol cosolvent system exhibits the largest density dependence. In all cases, the lowest concentration of added cosolvent results in a larger density effect on the equilibrium constant than the corresponding higher cosolvent concentrations. At the lowest cosolvent concentrations, miscibility limits permit the experiment to extend into the near-critical region of pure SCF ethane where local composition enhancements due to solute-solvent or solute-solute clustering are significant. At the higher concentrations, the experiments are further removed from this near-critical, compressible region. In addition, the shift in equilibrium constant towards the keto tautomer in the lower density regions may be enhanced by the reduction in self-association of the alcohols which occurs in this same region. These free alcohols have a greater tendency to form intermolecular hydrogen bonds with the keto tautomer.

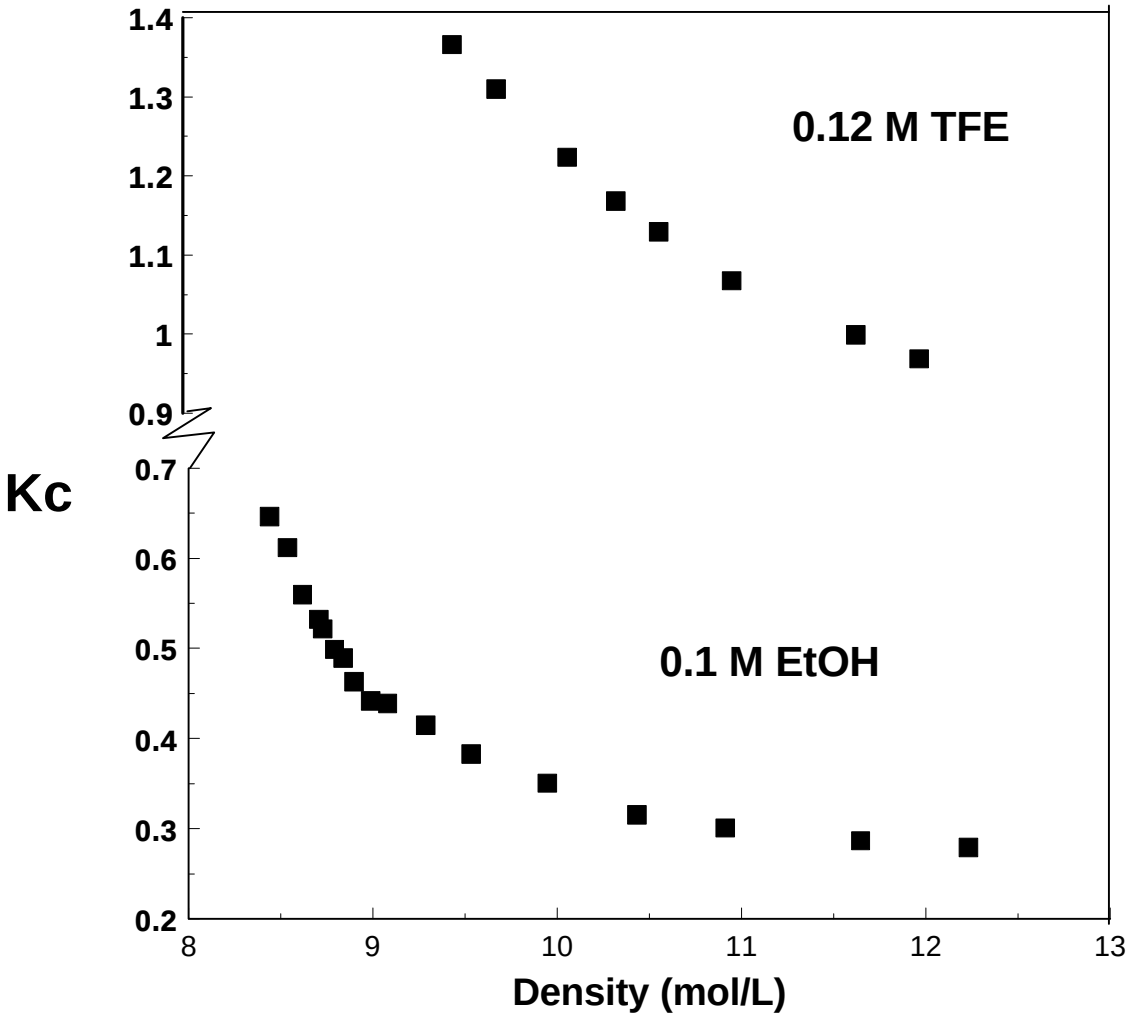

Figure 6. Equilibrium constant (K_c) as a function of density in cosolvent/SCF ethane in 0.1 M ethanol and 0.12M (Equilibrium constant (K_c) as a function of density in several cosolvent/SCF ethane systems.)

Therefore, the density effect observed can be attributed to a combination of factors. First, even in a compressed gas far from its critical point, density changes cause shifts in chemical equilibria due to changes in fugacity. However, in the near critical fluids we also have large effects due to local density and composition enhancements. Finally, hydrogen bonding of the keto tautomer to the cosolvent prevents tautomerization back to the enol form. As pressure is increased beyond the critical region, the equilibrium constant

of hydrogen bonding decreases (Gupta et al., 1993; Kazarian et al., 1993a; Kazarian et al., 1993b), which would reduce the concentration of the hydrogen bonded keto form and result in a decrease in the equilibrium constant.

Modeling Based on General Chemical Physical Analysis

A physical-chemical model has been developed to characterize the behavior of the equilibrium constant as a function of density. Possible equilibria describing this solute in a cosolvent modified solvent system are shown below. The equilibrium constant K_1 is the actual tautomerization between the keto and enol forms of the Schiff base. The equilibrium constants K_2 and K_3 indicate the equilibrium between the cosolvent, a hydrogen bond donor, and the Schiff base tautomers which are hydrogen bond acceptors, along with the hydrogen bonded complex of each form. Finally K_4 is the equilibrium constant for the dimerization of the alcohol cosolvents. Other equilibria such as the formation of the higher self-associates of the alcohol cosolvents are neglected. In addition, HFIP exists in an equilibrium between two rotamer forms which have slightly different acidities. This equilibrium is know to vary with density (Kazarian and Poliakoff, 1995), however, should have negligible effects on the Schiff tautomerization and will be ignored.

$$\begin{aligned} K &\overset{K_1}{\leftrightarrow} E \\ K + H &\overset{K_2}{\leftrightarrow} KH \\ E + H &\overset{K_3}{\leftrightarrow} EH \\ H + H &\overset{K_4}{\leftrightarrow} HH \end{aligned} \tag{3}$$

Where K , E, and H designate the keto tautomer, enol tautomer, and cosolvent, respectively.

For simplification, only cosolvent systems with minimal self-association were modeled. The self association of fluorinated alcohols such as TFE is minimal, and with HFIP, there is essentially no dimerization at the concentrations used (Schrems et al., 1992; Kazarian et al., 1993b; Marco et al., 1994). Additionally, it was found from gas phase hydrogen bonding data between the fluoro-alcohols and various ketonic and enolic (phenolic, in particular, such as the enol form of the Schiff base used in this investigation) compounds that the third equilibrium (K_3) may be ignored (Abraham, 1993; Marco et al., 1994) because the equilibrium constant for hydrogen bonds between fluoro-alcohols and ketones is so much greater in comparison to that between the fluoro-alcohols and the phenolic compounds. This results in a model based on only two equilibrium constants:

$$K_1 = \frac{z_K \phi_K}{z_E \phi_E} \tag{4}$$

$$K_2 = \frac{z_{KH} \phi_{KH}}{z_K \phi_K z_H \phi_H} \tag{5}$$

where z_K, z_E, and z_{KH} are the true concentrations of the keto and enol tautomers of the Schiff base, respectively, and the keto hydrogen bonded complex; and the ϕ_K, ϕ_E, and ϕ_{KH} are the fugacity coefficients for these species.

In order to compare the model directly to the experimental results, an expression in terms of the experimental equilibrium constant was derived. For this derivation, it was assumed that the fugacity coefficients for each of the free Schiff tautomers (ϕ_K and ϕ_E)

were equal and the free cosolvent concentration was constant, because in all cases the added cosolvent was in great excess of the Schiff base concentration. Then, the experimental equilibrium constant is given by,

$$K_{C,\exp} = \frac{\left[c_K + c_{KH}\right]}{\left[c_E\right]} \tag{6}$$

where the concentration of the keto tautomer is now a combination of the free and hydrogen bonded form of the tautomer. Then, the equilibrium constant calculated from a physical-chemical analysis becomes,

$$K_{C,calc} = K_1(1 + K_2 C_{\cos} \mathsf{f}^{*}) \tag{7}$$

where

$$\mathsf{f}^{*} = \frac{\mathsf{f}_K \mathsf{f}_H}{\mathsf{f}_{KH}}, \tag{8}$$

K_1, K_2 are defined previously in equations 4 and 5, and C_{cos} is the bulk cosolvent concentration.

The fugacity coefficients were calculated from the Peng-Robinson equation of state (Reid et al., 1987). The binary interaction parameters (k_{12}) for the cosolvent/ethane systems were regressed from measured mixture densities and are given in Table 2. The binary interaction parameters for the cosolvent/Schiff complex in SCF ethane (k_{14}) arbitrarily were set equal to those for the cosolvent The binary interaction coefficient for the Schiff base/ SCF ethane (k_{13}) were set equal to 0.1 and all other interaction parameters were set equal to zero. The critical properties of ethane, ethanol (Reid et al., 1987), and TFE (Suresh et al., 1994) were obtained from the literature. The critical temperatures of HFIP, Schiff base, and Schiff base/cosolvent hydrogen bonded complex were estimated

from Fedor's method; the critical pressure and volume for the same compounds were estimated using the Joback method; and the acentric factor was estimated from the critical volume (Reid et al., 1987).

Table 2. Binary interaction parameters for SCF ethane/cosolvent systems regressed from experimental data using the Peng-Robinson equation of state.

Cosolvent in SCF Ethane	**Cosolvent Composition (mol%)**	**k_{ij}**
TFE	0.98	0.055
TFE	1.98	0.194
HFIP	0.68	-0.053
HFIP	1.36	0.033
EtOH	1.7	0.061

The equilibrium constant for the Schiff base keto tautomer/cosolvent hydrogen bonded complex (K_2) was assumed to be equal to the gas phase equilibrium constant for the same hydrogen bond donors with similar ketone compounds . These were obtained from the literature (Marco et al., 1994) and are given in Table 3. The gas phase data were given for 25 °C and were corrected to experimental conditions of 35 °C using gas phase enthalpy of formation literature data for the appropriate cosolvent/ ketone complex (Kivinen and Murto, 1969; Tucker and Christian, 1976). The equilibrium constant of tautomerization for the free Schiff base in the keto and enol forms was fit to the experimental data at the highest pressure data to avoid the effect of the anomalous behavior associated with the SCF critical region is absent.

Table 3. Equilibrium constants (K_2) for keto Schiff base/cosolvent hydrogen bonded complex at 25°C and corrected to 35°C.

Schiff Base/Cosolvent Hydrogen Bonded Complex	**K_2 (L/mol) 22°C**	**K_2 (L/mol) 35°C**
TFE	53	37
HFIP	250	154

The results of the model for the highest and lowest cosolvent concentration of TFE and HFIP are shown in Figures 7 and 8. With both cosolvent systems, the model agrees with the experimental data much better at the highest cosolvent concentration. In all cases, however, the model diverges from the experimental data in the area closest to the critical region. The model takes into account the changes in the K_C which result from changes in solution fugacity. Therefore, it is likely that the differences between the theory and the experimental data are a result of solute-cosolvent clustering resulting from local composition enhancements and increases in hydrogen bonding approaching the critical region.

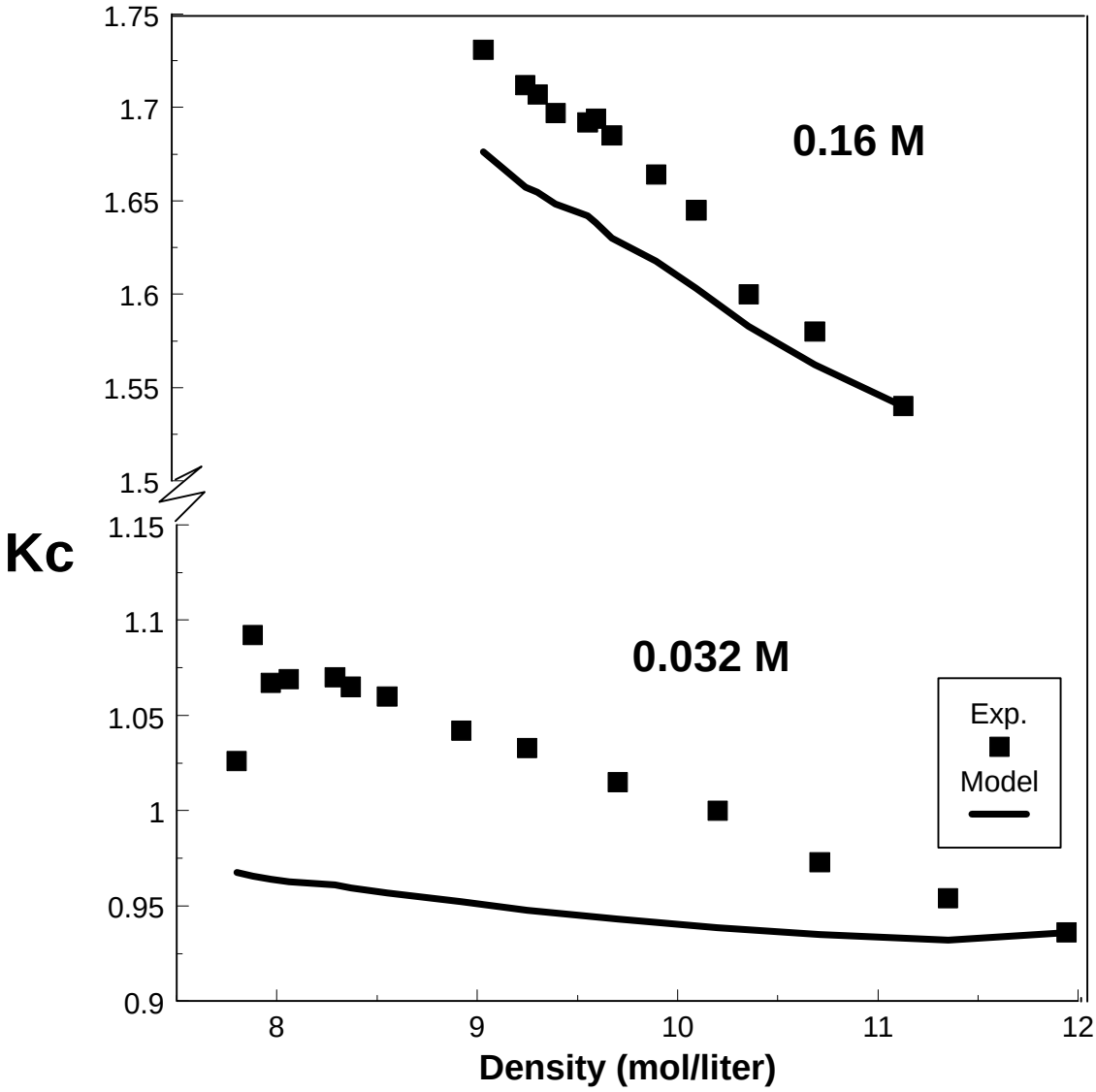

Figure 7. Results of equilibrium model:) 0.046 M and 0.24 M TFE/SCF ethane at 35°C. (Results of equilibrium model for Schiff base in TFE/SCF ethane solvent system.)

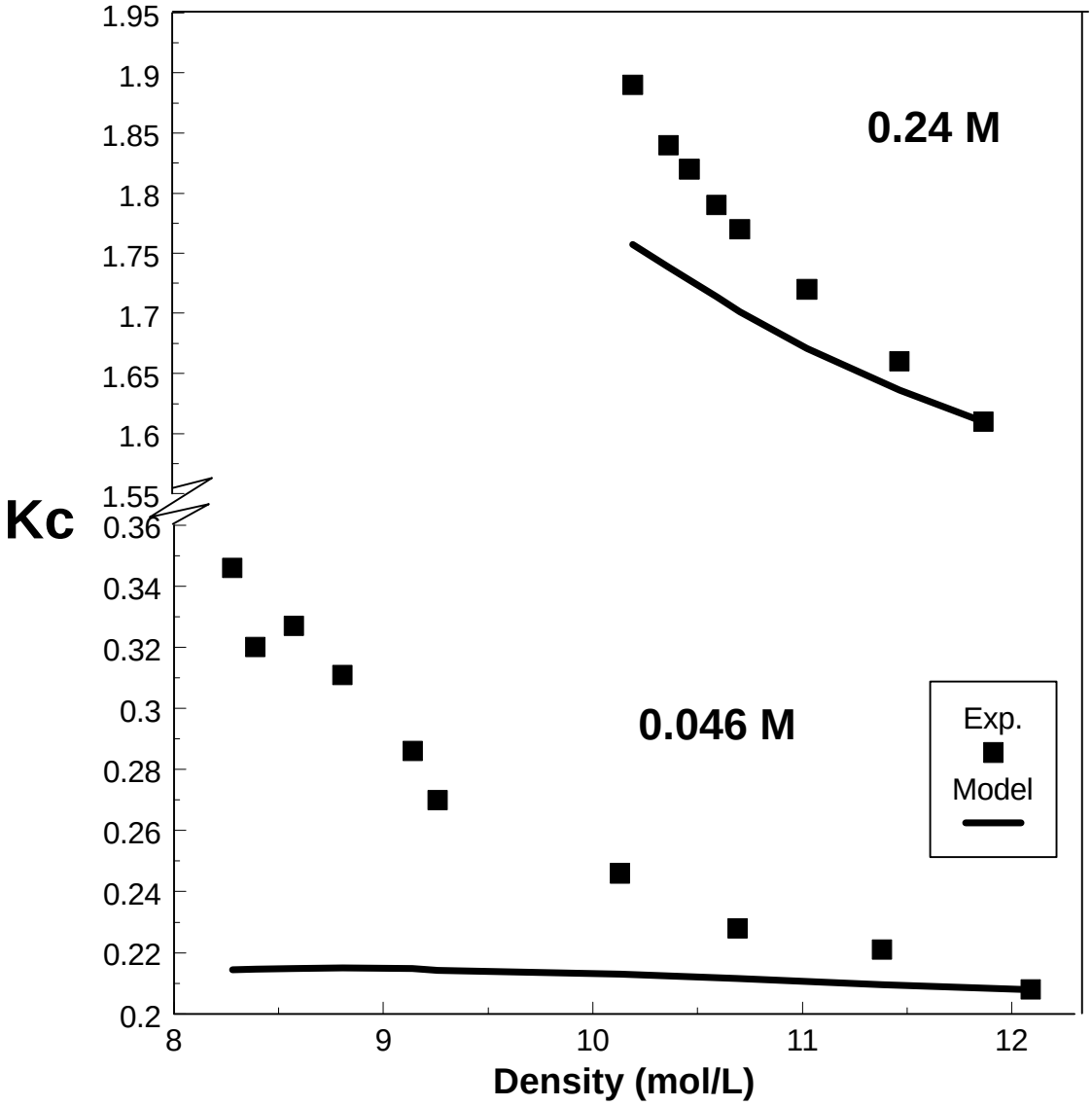

Figure 8. Results of equilibrium model: 0.032 M and 0.16 M HFIP/SCF ethane at 35°C. (Results of equilibrium model for Schiff base in HFIP/SCF ethane solvent system.)

A sensitivity analysis of the variables associated with the prediction of the equilibrium constant was performed to ensure that the differences between predicted and experimentally measured data were not due to inaccuracies in estimated values and literature constants. From the perturbation of estimated and literature values, it was found that the only variable in the model which could account for the magnitude of the

discrepancy between the model and experiment was the cosolvent concentration. The local concentration of cosolvent needed for the model and experimental data to agree at the lowest density point for each data set is given in Table 4. The local composition enhancement needed for this local concentration is also given in this table. For both cosolvent/SCF systems modeled, the local concentration of cosolvent around the Schiff base is equal (within experimental error) for the highest and lowest bulk cosolvent concentrations. This is consistent with the possibility of saturation of the local cosolvent concentration about the Schiff solute.

Table 4. Local composition enhancement and local concentration of cosolvent about the Schiff base from modeled results using chemical-physical theory.

Cosolvent	Bulk Concentration (M)	Mole Fraction Ratio x_{local}/x_{bulk}	Local Concentration (M)
TFE	0.046	9.2	0.423
TFE	0.24	1.7	0.401
HFIP	0.032	6.5	0.208
HFIP	0.164	1.3	0.213

There are several possible explanations for the observations above. At the highest cosolvent concentrations, miscibility limits dictate that the experiments are carried out beginning at densities which are well removed from the near critical region of the solvent system. In the cases of the lowest cosolvent concentrations, it was possible to extend the spectroscopic measurements into the critical region of the solvent system without phase splitting, where local composition enhancements are known to occur. In addition, with

nearly 2 mol% of added cosolvent, the fluid is much less compressible in general than at lower cosolvent concentrations. It is also known that the equation of state fugacity coefficient calculations are more accurate at pressures well removed from the critical region.

II) DIELS-ALDER REACTION OF ANTHRACENE AND PTAD

Over the last two decades, supercritical fluids have received an increasing amount of attention as a medium for carrying out chemical reactions (Savage, et al., 1995). The interest stems from unique advantages that supercritical fluids provide in the area of reaction rate control. A supercritical fluid, defined as a material at conditions above its critical temperature and pressure, is highly compressible at conditions near its critical point. The compressibility of the solvent can lead to large changes in reaction rate over small changes in pressure, and since pressure can be manipulated easily and precisely, pressure tuning represents a convenient route to rate control. Additional control of reaction rate can often be achieved through modification of the supercritical solvent with small amounts of a second solvent, designated as a cosolvent.

Among supercritical solvents, CO_2 has received special attention due to the fact that, in addition to a density which can easily be tuned over an order of magnitude, it also provides a compelling combination of low cost, an easily accessible, thermally mild critical point, and low toxicity. This combination of attributes is especially attractive to the food and pharmaceutical industries.

The reactants used to produce the rate data in this work follow a Diels-Alder reaction pathway, but the dienophile, 4-phenyl-1,2,4-triazoline-3,5-dione (PTAD), is atypical. The reactive part of PTAD's structure is identical to maleimide, but has a pair of nitrogens at the bonding site instead of carbons. The reaction is illustrated in Figure 9. The nitrogen substitution results in reaction rates an order of magnitude higher than

maleimide (Konovalov, et al., 1979), and has allowed the data presented in this work to be collected relatively swiftly. PTAD possesses another attractive aspect in addition to its high reactivity, and that is the fact that, as a member of the Diels-Alder class of reactions, it is an elementary, bimolecular reaction with a well established mechanism (Sauer, 1967). This allows the rate constant to be measured using simple pseudo first order data reduction techniques.

Figure 9. The Diels-Alder reaction of anthracene (diene) with 4-phenyl-1,2,4-triazoline-3,5-dione (dienophile.)

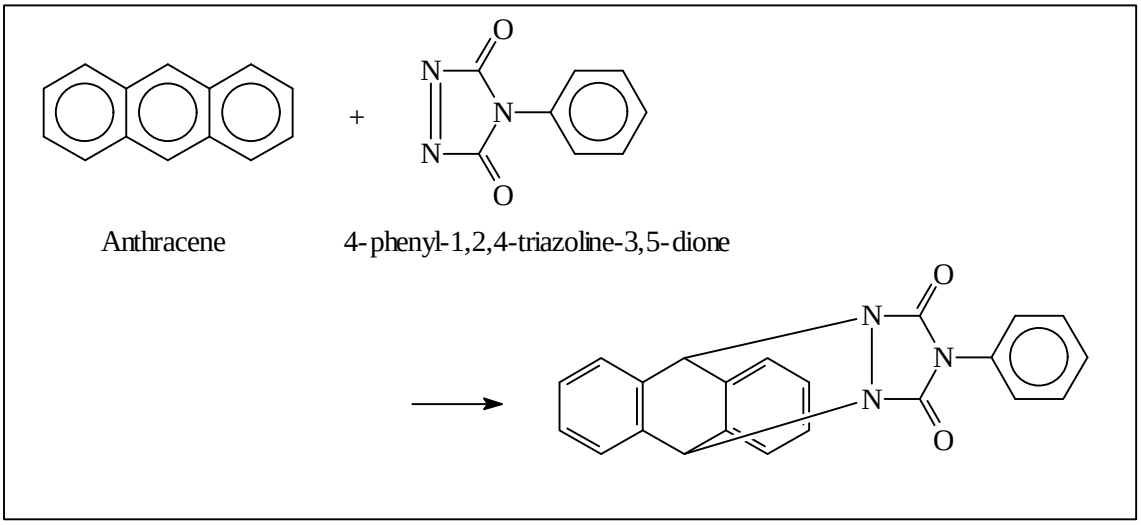

PROCEDURE

Reaction kinetics were followed spectroscopically by fluorescence. The equipment used to make these measurements was configured in the manner illustrated in Figure 10. Light from a Spectral Energy SX1000-2 Xenon UV lamp was passed through a Kratos

Analytical Model GM252 monochromator, producing an excitation light beam

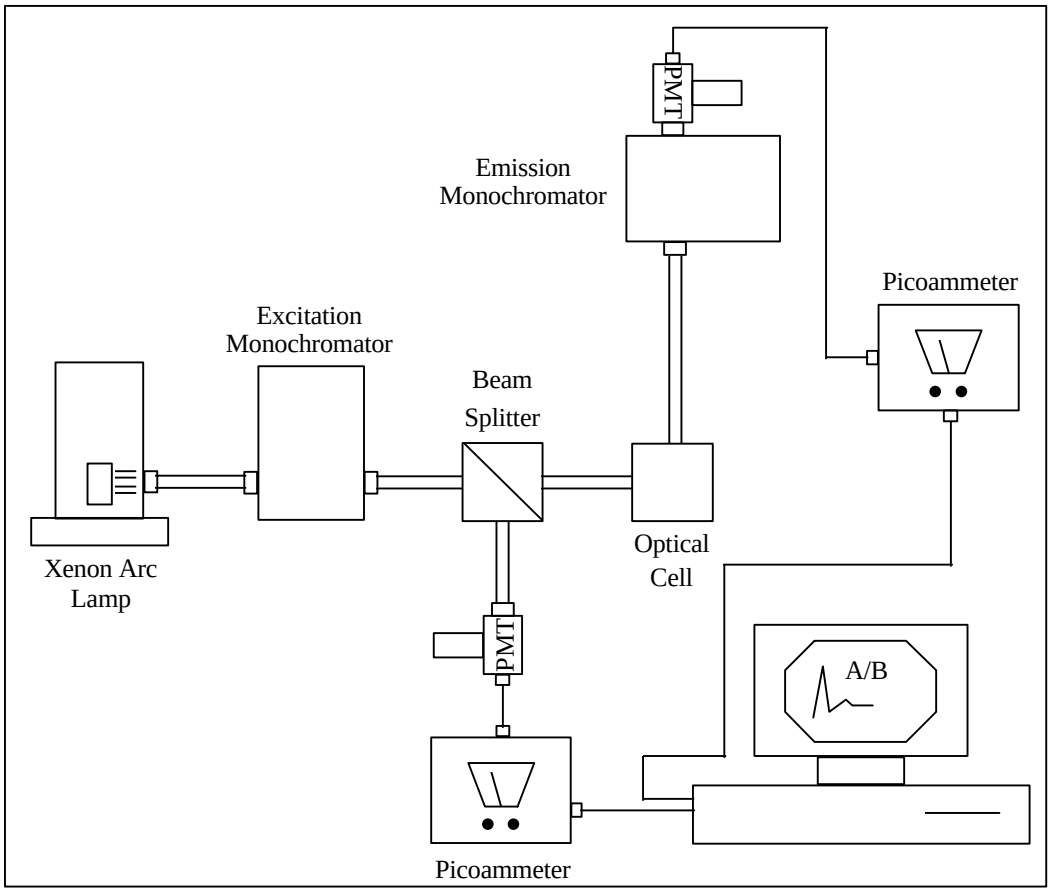

Figure 10. An overview of the high pressure fluorescence apparatus used for kinetic measurements.

at a single wavelength. The excitation beam was split into two beams using a half-silvered mirror, producing an excitation beam and a reference beam.

The reference beam was directed into a Kratos D 500 Side-On Photomultiplier Tube (PMT), which produced an amperage output measured using a Keithley Instruments 414A Picoammeter. The excitation beam was directed into the optical cell containing the experimental sample of anthracene. The fluorescence of anthracene produced an emission beam of light, which was directed into a second GM252 monochromator where it was

filtered to a single wavelength of light. The filtered emission wavelength was directed into a second D 500 PMT, which produced an amperage output that was measured using a Keithley 485 Autoranging Picoammeter.

Each picoammeter produced an analog output voltage in proportion to beam intensity, designated as Signal A for the emission beam intensity and as Signal B for the reference beam intensity. The ratio of these two signals - A/B - varied with changes in fluorescent emission intensity, but it did not vary with fluctuations in lamp intensity. The emission intensity of the sample was recorded as the numerical value of the ratio A/B.

The optical cell was constructed from 316 stainless steel and was configured for solvent introduction and removal as in Figure 11. The windows were made from quartz, and were positioned at right angles to one another so that as little of the excitation light as possible would exit the cell with the emission light. The seals for cell windows were o-rings made of Teflon. All tubing and fittings were stainless steel and were manufactured by Swagelok or HiP. CO_2 was delivered to the cell using an ISCO Model 260D syringe pump, which fed through a Valco 6-port sample injection valve. A Teflon coated stirbar was used to provide agitation of the cell contents.

Pressure was measured using a Druck PDCR 911 transducer attached to a Druck DPI 60 digital readout. The pressure transducer and readout were calibrated using a Ruska dead weight calibration apparatus, and were found to be accurate to +/- 1 psi.

Internal temperatures were measured using a 1/16” grounded Omega Type K thermocouple in an inconel sheath. It was mounted with its tip in direct contact with the reactant solution. The thermocouple was attached to a readout with resolution to 0.1ºC.

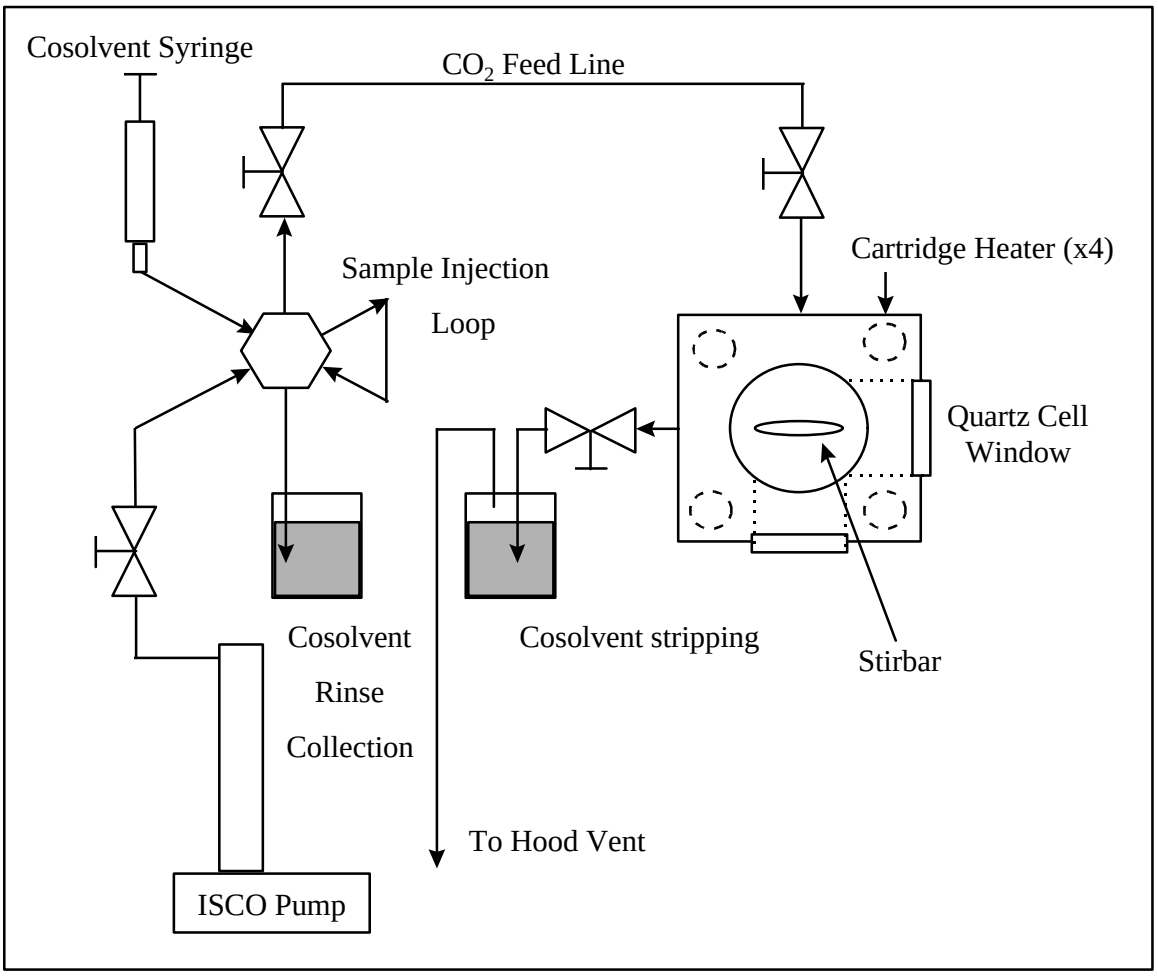

Figure 11. An overview of the optical cell and the apparatus used for the injection of cosolvents.

The thermocouple was calibrated against a platinum resistance thermometer, and was found to be accurate to +/- 0.1ºC.

Internal temperature was controlled using a second 1/8" Type K thermocouple mounted with its tip in the steel of the cellblock. The thermocouple was attached to an Omega CN9000A controller which used four cartridge heaters mounted in the steel of the cell block to maintain cell temperature. Temperature control of cell contents was within +/- 0.2ºC.

Kinetic Analysis

The reaction of PTAD with anthracene is an elementary bimolecular reaction, so, if one reactant is present in excess, pseudo first order kinetics can be used to extract rate constants from concentration versus time data. UV spectroscopy was used for the analysis of the reaction rate of PTAD and anthracene in liquid solvents (Konovalov, Breus et al. 1979) by following the decay of PTAD over time. In order to apply pseudo first order kinetics, anthracene needs to be present in excess. Though an excess of anthracene is possible in liquids, PTAD solubility in supercritical CO_2 is on the order of 10^{-3} mol/L, and anthracene solubility is on the order of only 10^{-5} mol/L. The dilemma was solved by using fluorescence spectroscopy instead of UV. Fluorescence spectroscopy can detect concentrations of anthracene as low as 10^{-7} mol/L, making it possible to have PTAD present at an initial excess of 100:1 and still follow a change in anthracene concentration over two orders of magnitude.

In order to calculate the rate constant of the reaction conveniently from fluorescence emission data, it was possible to use Beer's law to relate pseudo first order rate constants directly to changes in emission signal. Solution of the differential equation (9) relating concentration changes of one reactant to the concentration of both reactants leads to (10) when PTAD is assumed to be in great excess and therefore constant throughout the reaction.

$$\frac{dc_{AN}}{dt} = k_c c_{PTAD} c_{AN} \qquad (9)$$

$$\ln\left(\frac{c_{AN}}{c_{ANo}}\right) = -\left(k_c c_{PTADo}\right)t \quad (10)$$

Simple experiments involving incremental additions of anthracene to a liquid solvent indicated that the fluorescence of anthracene follows Beer's Law (11) as long as the anthracene is dilute (i.e. less than 10^{-5} mol/l), and the emission wavelength monitored is well removed from wavelengths at which self-absorption may occur. The path length "l" in Beer's Law does not change during a run, so (11) may be written once for initial conditions and again for an arbitrary time t. The ratio of these equations may be substituted into (10), leading to (12). Equation (12) allows the pseudo first order rate constant to be derived directly from emission data without knowing the exact concentration of anthracene in the cell.

$$e = \varepsilon l c_{AN} \tag{11}$$

$$\ln\left(\frac{e_{AN}}{e_{ANo}}\right) = -k_c c_{PTADo} t \tag{12}$$

Kinetic Measurements in Pure Supercritical CO_2

Stock solutions of PTAD and anthracene were prepared in acetone. A fresh PTAD stock solution was prepared each day. A known quantity of each stock solution was placed into the optical cell using a Gilman Pipet, with PTAD in excess by a factor of 40. The cell was dried under vacuum for 5 minutes. Care was taken to insure that the two stock solutions did not contact one another during drying. Dryness of the cell was determined by visual inspection.

Data acquisition software was started, and the cell was pressurized with pure CO_2 from the ISCO syringe pump. The time and pressure at which the cell reached the desired temperature was recorded, and the reaction was observed for about twenty minutes. Kinetic analysis was performed only on data collected while the cell was at within +/- 0.2ºC of the desired temperature. The cell was cleaned thoroughly with acetone between each experiment.

Modeling of Kinetic Data in Pure Supercritical CO_2

Rate constants were previously obtained for the reaction in pure CO_2 at 40ºC and at pressures ranging from the critical pressure of CO_2 (73.8 bar) to 216 bar. Rate constant

values are plotted in Figures 12 and 13. Two views are provided for the purpose of making the cluster of points at 95 bar more readable. Near the critical temperature, the reaction shows great sensitivity to pressure in the region between the critical pressure and about 110 bar. Rate constants at the critical pressure are as much as 26 times greater than those above 110 bar. The average estimated error in rate constant values was 20% at higher pressures, increasing to as much as 70% near the critical pressure.

The drop in rate constant with increasing pressure is similar to the result obtained for the esterification of phthalic anhydride with methanol in supercritical CO_2 [Brennecke, et al, 1994]. The bimolecular rate constant for the phthalic anhydride reaction also decreased at pressures above the critical pressure and produced rate constant enhancements near the critical pressure similar in magnitude to those observed for the PTAD reaction. Brennecke estimated the local concentration of methanol around a phthalic anhydride molecule using an analogy with solvatochromic work using phenol-blue [Johnston, 1987 #58]. She determined that, in the region near the critical pressure, local concentration was higher than bulk concentrations by a factor of 5. When this increase in local concentration was accounted for, and rate constants were calculated using local concentration values, the reaction showed only a slight sensitivity to pressure in the region near the critical pressure.

Figure 12. Rate constants for the reaction of PTAD with anthracene in pure CO_2 at 40°C.

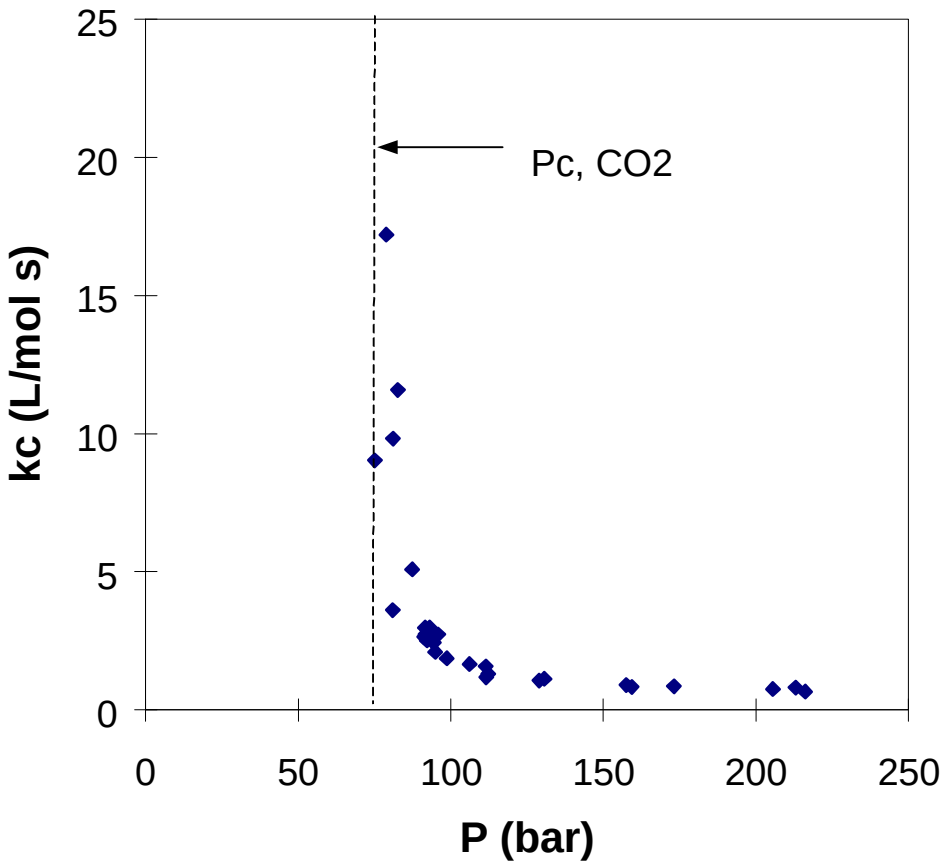

Figure 13. Rate constants having values less than 5 l/mol s for the reaction of PTAD with anthracene in pure CO_2 at 40°C.

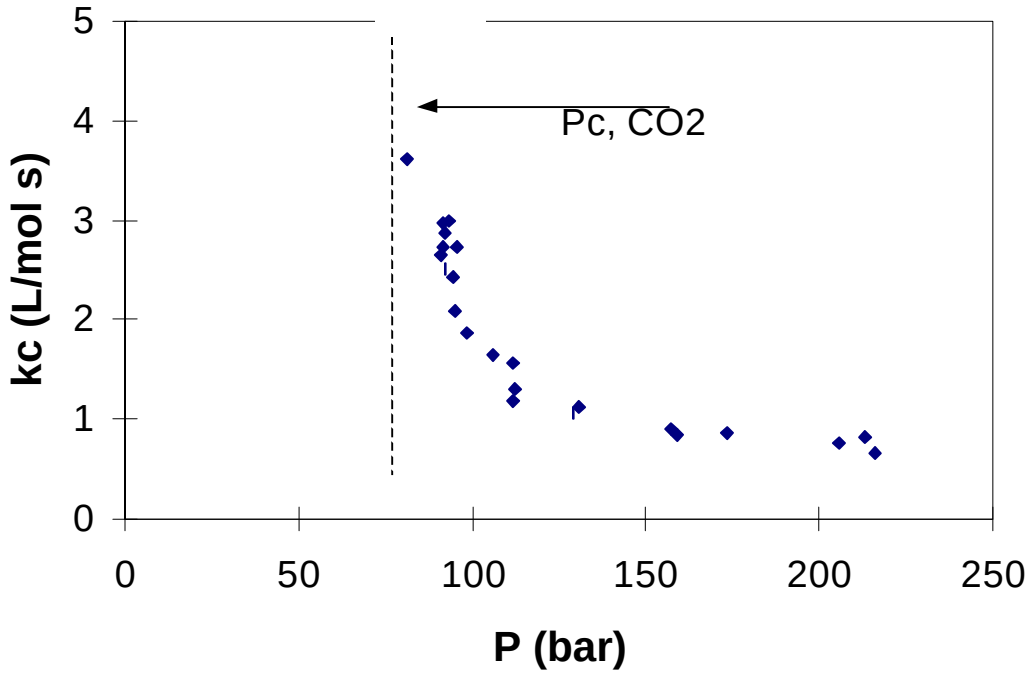

In order for a local concentration increase to occur in the reaction of PTAD with anthracene, it is necessary for solute-solute clustering to be present along with solute-solvent clustering. Evidence for solute-solute clustering in dilute solutions is found in work by Kurnik [Kurnik, 1982 #98], so clustering effects on local concentrations are one possible explanation of the rate constant trends found in this work.

The construction of mathematical models capable of predicting these kinetic changes is now underway. The simplest promising avenue of investigation involves the assumption that the clustering effects are minimal, and that the kinetics may be successfully modeled as a function of changes in bulk fluid properties. The supercritical CO_2 can then be treated as a dense gas, which allows the following kinetic model based on high reference pressure fugacity coefficients to be derived (Eckert, 1974).

$$\frac{k}{k_o} = \frac{f_A f_B z}{f_M} \qquad (13)$$

Here, $f's$ are fugacity coefficients, and z is the usual compressibility factor of the gaseous mixture. Currently, a computer program for evaluating these fugacity coefficients at arbitrary pressures is being written. Evaluation of the fugacity coefficient model against experimental data using this program will continue into the next quarter.

Kinetic Data in Pure Supercritical CO_2 at 50°C

Rate constants were obtained for the reaction of PTAD with anthracene in pure CO_2 at 50ºC and at pressures ranging from the critical pressure of CO_2 (73.8 bar) to 195

bar. Rate constant values at both 40°C and 50°C are plotted in Figure 14. At 40°C, the reaction shows great sensitivity to pressure in the region between the critical pressure and about 110 bar. Rate constants at the critical pressure are 25 times greater than those above 110 bar. At 50°C, the reaction rate constant shows only a slight change with pressure around the critical pressure. This slight increase in rate as pressure decreases is predicted by transition state theory (Evans and Polanyi, 1935; Brennecke, et al, 1994). The modest rate constants near the critical pressure indicate that molecular clustering is minimal at this temperature.

.

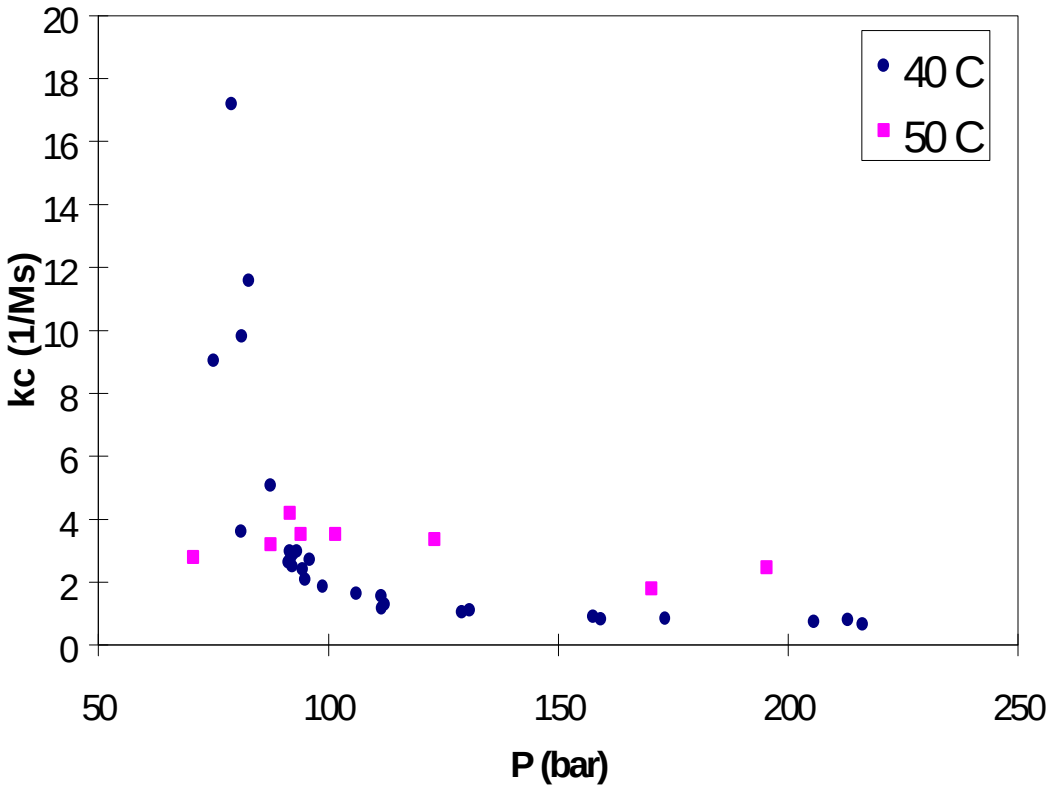

Figure 14. Rate constants for the reaction of PTAD with anthracene in pure CO_2 at 50^{o}C.

CONCLUSION

Densities of binary supercritical mixtures of ethane with cosolvents, ethanol, 2,2,2-trifluoroethanol, and 1,1,1,3,3,3-hexafluoro-2-propanol, have been measured by a constant volume apparatus. Measurements were made in the range 0.7 to 2.0 mol % cosolvent and pressure from 49.8 to 105.7 bar at 308.2 K. The tautomeric equilibrium constant was measured as a function of density in supercritical ethane modified with three different concentrations of hexafluoroisopropanol (HFIP). The measured equilibrium constant was found to be a function of fluid density and cosolvent concentration.

The position of Schiff base tautomeric equilibria was tuned from essentially one tautomer to another by modifying the solvent of pure SCF ethane with less than 2 mol% of cosolvents capable of hydrogen bonding interactions. For the cosolvents of EtOH, TFE, and HFIP, it was found that the equilibrium constant was a function of cosolvent concentration and mixture density. Modeling the equilibrium constants using general chemical-physical analysis results in differences in predicted and experimentally calculated equilibrium constants which are greater than accountable by theory alone. This evidence of solute-cosolvent clustering is consistent with the effects of density on hydrogen bonding (Kazarian et al., 1993). Hydrogen bonding has been shown to decrease with increasing density. A local composition enhancement of cosolvent about the Schiff base in the low density, near-critical region would result in an increased amount of hydrogen bonding which in turn shifts the equilibria to the keto tautomer. As the density of the solution is increased, the solute-cosolvent clustering decreases as the fluid becomes less compressible which also reduces the degree of hydrogen bonding. This decrease in

hydrogen bonding in turn affects the keto-enol equilibria by decreasing the amount of the keto formation. Thus, it is possible to utilize density dependence of hydrogen bonding in SCF solutions to "tune" tautomeric equilibrium between the keto-enol forms of the Schiff base.

Kinetic Diels-Alder data have been collected for pure CO_2 at 40^{o}C and pressures between the critical pressure of CO_2 (73.8 bar) and 216 bar. These data support the theory of local density enhancements suggested in the literature. Data taken at 50^{o}C and pressures ranging from 70 bar to 195 bar are also reported; they do not exhibit the molecular clustering evident closer to the critical temperature.

REFERENCES

Abraham, M. H. *Chemical Society Reviews*, 73 (1993).

Bjerrum, N., *Z. Physik. Chem.*, **108**, 82 (1924).

Brennecke, J. F.; Eckert, C. A. *AIChE. J.*, **35**, 1409 (1989).

Brennecke, J.F., Ellington, J.B., and Park, K.M., *Ind. Eng. Chem. Res.*, **33**, 965 (1994).

Brennecke, J.F., Tomasko, D.L., Peshkin, J., and Eckert, C.A., *Ind. Eng. Chem. Res.*, **29**, 1682 (1990).

Bronsted, J.M., *Z. Physik. Chem.*, **102**, 169 (1922).

Clifford, T. and Bartle, K., Chemical Reactions in Supercritical Fluids, 1996.

Eckert, C.A., *I&EC*, **59**, 20 (1967).

Eckert, C.A. and Knutson, B.L., *Fluid Phase Equilibr.*, **83**, 93 (1993).

Ely, J.; Bruno, T. J. *Supercritical Fluid Technology: Reviews of Modern Theory and Applications*; Ely, J.; Bruno, T. J., Ed.; CRC Press: Boston, 1991.

Ely, J.F., Haynes, W.M., and Bain, B.C., *J. Chem. Thermodynamics*, **21**, 879 (1989).

Evans, M.G. and Polanyi, M., *Trans. Faraday Soc.*, **31**, 875 (1935).

Eyring, H., *J. Chem. Phys.*, **3**, 107 (1935).

Gupta, R. M.; J. R. Combes; and K. P. Johnston, "Solvent Effects on Hydrogen Bonding in Supercritical Fluids," *J. Phys. Chem.*, **97**, 707, (1993).

Hildebrand, J.H. and Scott, R.L., Regular Solutions; Prentice-Hall: Englewood Cliffs, NJ, 1962.

Hughes, E.D. and Ingold, C.K., *J. Chem. Soc.*, 244 (1935).

Ikushima, Y., Ito, S., Asano, T., Yokoyama, T., Saito, N., Hatakeda, K., and Goto, T., *J. of Chem. Eng. In Japan*, **23**, 96 (1990).

Isaacs, N.S. and Keating, N., *J. Chem. Soc., Chem. Commun.*, 876 (1992).

Johnston, *Chem. Eng. Comm.*, **63**, 49 (1988).

Johnston, K.P., Ziger, D.H., and Eckert, C.A., *Ind. Eng. Chem. Fundam.*, **21**, 191 (1982).

Johnston, K. P.; Penninger, J. M. L. *Supercritical Fluid Science and Technology*; Johnston, K. P.; Penninger, J. M. L., Ed.; ACS: Washington, DC, 1989.

Kazarian, S. G.; Hamley, P. A.; Poliakoff, M. *J. Amer. Chem. Soc.*, **115**, 9069 (1993).

Kazarian, S. G.; R. B. Gupta; M. J. Clarke; K. P. Johnston; and M. Poliakoff. *J. Amer. Chem. Soc.*, **115**, 11099 (1993a).

Kazarian, S. G. and M. Poliakoff. *J. Phys. Chem.*, **99**, 8624 (1995).

Kim, S. and Johnston, K.P., *AIChEJ*, **33**, 1603 (1987a).

Kim, S. and Johnston, K.P., *Ind. Eng. Chem. Res.*, 1206 (1987b).

Kivinen, A.; and J. Murto. *Suomen Kemistilehti*, **B**, 190 (1969).

Konovalov, A.I., Breus, I.P., Sharagin, I.A., and Kiselev, V.D., *Zhurnal Organicheskoi Khimii*, **15**, 361 (1979).

Laidler, K. Chemical Kinetics; Third ed.; Harper Collins Publishers, Inc.: New York, 1987a.

Laidler, K. Chemical Kinetics; Third ed.; Harper Collins Publishers, Inc.: New York, 1987b.

Marco, J.; J. M. Orza; R. Notario; and J.-L. M. Abboud. *J. Am. Chem. Soc.*, **116**, 8841 (1994).

Paulaitis, M.E. and Alexander, G.C., *Pure and Appl. Chem*., **59**, 61 (1987).

Reid, R. C.; J. M. Prausnitz; and B. E. Poling, *The Properties of Gases & Liquids*, McGraw-Hill: New York, (1987).

Salman, S. R.; Farant, R. D.; Lindon, J. C. *Spectroscopy Letters*, **24**, 1071 (1991).

Sauer, J., *Angew. Chem. Internat. Edit*., **6**, 16 (1967).

Savage, P.E., Gopalan, S., Mizan, T.I., Martino, C.J., and Brock, E.E., *AIChEJ*, **41**, 1723 (1995).

Schrems, O.; H. M. Oberhoffer; and W. A. P. Luck. *J. Phys. Chem.*, **88**, 4335 (1984).

Tomasko, D. L. *Spectroscopic and Thermodynamic Studies of Supercritical Fluid Solutions Containing a Cosolvent*; Tomasko, D. L., Ed.; University of Illinois: Urbana-Champaign, 1992.

Tucker, E. E.; and S. D. Christian. *J. Am. Chem. Soc.*, **98**, 6109 (1976).

Weinstein, R.D., Renslo, A.R., Danheiser, R.L., Harris, J.G., and Tester, J.W., *J. Phys. Chem.*, **100**, 12337 (1996).

Yagi, Y.; Saito, S.; Inomata, H. *J. Chem. Eng. Japan*, **26**, 116 (1993).

Yamasaki, K.; Kajimoto, O. *Chem. Phys. Lett.*, **172**, 271 (1990).

Yun, S. L. J.; Dillow, A. K.; Eckert, C. A. *J. Chem. Eng. Data*, **41**, 791 (1996).